Post-Print

This is the accepted version of:

A. Grande, S.J. Garcia, S. Van Der Zwaag
On the Interfacial Healing of a Supramolecular Elastomer
Polymer, Vol. 56, 2015, p. 435-442
doi:10.1016/j.polymer.2014.11.052

The final publication is available at https://doi.org/10.1016/j.polymer.2014.11.052

On the interfacial healing of a supramolecular elastomer

A. M. Grande*, S. J. Garcia, S. van der Zwaag

Novel Aerospace Materials, Faculty of Aerospace Engineering, Delft University of Technology, Kluyverweg 1, 2629 HS, Delft, the Netherlands.

*e-mail corresponding author: a.m.grande@tudelft.nl

Keywords: self-healing, supramolecular elastomer, fracture.

Abstract

In this work the self-healing behaviour of a supramolecular elastomer showing healing at room temperature was studied by mechanical testing. Tensile experiments on pristine and healed samples were conducted and a critical analysis of the material response under the testing conditions applied pointed out that simple tensile test only allows a restricted quantification of the healing process. A fracture mechanics approach based on the J-integral was adopted to measure the healing behaviour across the restored interface between the original fracture surfaces. The processes involved in the repair were identified by combining the information obtained with the different techniques. A substantial improvement in the assessment of the interfacial healing was achieved.

1 Introduction

The field of self-healing polymers is rapidly developing and several healing concepts have recently been presented leading to the growth of this innovative material class with potential applications in various engineering sectors. The different approaches applied to create thermoplastic and thermoset polymers and elastomers can be separated into extrinsic and intrinsic concepts. In extrinsic concepts the self-healing response is achieved via the inclusion of dedicated discrete particles containing a so-called healing agents. In intrinsic healing approaches, the ability to heal is based on reversible chemical bonds intrinsically present in the material. These reversible bonds allow reformation of the mechanical integrity provided the original fracture surfaces are brought into contact for a sufficiently long time to allow adequate molecular motion across the interface. As the healing process does not consume any healing agent, in intrinsic healing systems samples can be broken and healed at the same place several times [1].

For intrinsic self-healing systems the polymer architecture plays a fundamental role and a sufficiently high chain mobility in combination with a sufficient density of reversible chemical bonds is a key requirement to obtain a material with the ability of single or multiple healing [2]. Systems showing extensive healing at room temperature or minimally raised temperature can be based on hydrogen bonding [3-5], disulphide bridges [6, 7], ionomers [8, 9] or other reversible bonds. More attractive mechanical properties while maintaining a sufficient self-healing behaviour can be obtained by blending intrinsically healing polymers with other stiffer and stronger polymers [10-12].

Elastomers, thanks to their flexible polymer network, are therefore ideal candidates for the design and the study of new self-healing concepts, including those arising from different supramolecular chemistries [13, 14]. Despite the significant potential for the development of self-healing elastomers the progress in the field is somewhat limited by the absence of established testing procedures capable of accurately quantifying healing efficiencies [15].

To date, tensile testing (in which a broken sample is reassembled in such a way that the fracture surfaces are brought in almost perfect contact and allowed to heal for a specified combination of

time, temperature and contact pressure prior to reloading of healed sample) forms the most common testing method and the aim is to find those conditions which restore the original tensile strength as much as possible. However, limited information can be extracted from this test procedure and the healing efficiencies depend strongly on sample size and perfection of the repositioning of the two original fracture surfaces during healing. Maes et al. [16] explored the healing behaviour of a hydrogen bonds based supramolecular rubbers through a tack-like experiment; in this study, the relevance of fracture/healing conditions and its impact on the degree of healing was clearly underlined. A peel test was selected by Rahman et al. [17] to investigate the self-adhesion assisted healing behaviour of epoxidized natural rubbers (ENR) highlighting the effects of contact time and temperature on the healing performance; a correlation between the healing capability exhibited by ENR based systems after high energy impacts and quasi-static damages was also proposed [18]. Finally, Keller et al. [19, 20] studied the healing response of an extrinsic microencapsulated polydimethylsiloxane (PDMS) elastomer system by both tear and torsion fatigue testing procedures.

More quantitative information on the healing behaviour across the interface between two former fracture surfaces can be obtained from test protocols based on fracture mechanics, as crack propagation can be considered an instructive case to investigate the interplay between polymer structure and mechanical properties [21-23] allowing a quantification of the material resistance to fracture in the presence of flaws or defects.

Early fracture mechanics studies on elastomers were performed by Rivlin et al. [24] extending the Griffith theory for crack growth in elastic materials to the case of vulcanized rubber and demonstrating how tear energy is strictly a material property independent by sample geometry. In recent years, the J-integral approach, introduced by Cherepanov [25] and Rice [26], has been widely applied to characterise the fracture properties of elastomers obtaining information on both the resistance to crack initiation and that to crack propagation [27-29].

In the present work, a fracture mechanics approach based on the application of the J-integral methodology is explored to investigate the self-healing behaviour of a hydrogen bond based supramolecular elastomer. The comparison between the healing performances measured by means of standard tensile and fracture experiments on virgin and healed samples revealed a different degree of recovery of original properties. The results obtained highlight the need to combine several experimental techniques such as mechanical, rheological and fracture microscopy measurements to unravel the various factors playing a role in the healing process and to obtain a more quantitative and objective determination of the degree of healing.

2 Experimental

2.1 Material and samples preparation

In the current study a commercial self-healing supramolecular elastomer previously documented in the literature was employed [4, 30-32]. The hybrid polymer network contains both strong irreversible covalent cross-links and weak reversible chemical bonds (hydrogen bonds).

The uncured version of the supramolecular elastomer was provided by Arkema and the samples were prepared following the manufacturers recommended procedure. The pre-polymer was heated at 90 °C and casted in a PTFE open mould (160 x 160 mm). Then, the mould was placed in a standard oven at 120 °C and vacuum was applied for 1 hour in order to allow outgassing of the resin. After vacuum release, the mould was closed with a PTFE cover to control the final sheet thickness (3±0.2 mm) and was kept in the oven for a further 23 hours. After cooling to room temperature, the square specimen was finally released from the mould.

Dog-bone (ASTM D1708) and single edge notched tensile (SENT) samples (80x25 mm), for tensile and fracture tests, respectively, were cut with shaped dies from the as-produced sheets. A fresh sharp razor blade was use to introduce a notch in each of the SENT specimens. A PTFE film was then

inserted into the notched zone of the SENT samples to avoid contact between the separated surfaces during the storage and healing phases.

All samples were stored in an environmental chamber at 23 °C and 20% RH for at least 24 hours prior to testing.

2.2 Testing procedures

Uniaxial tensile tests were performed on an Instron Model 3365 universal testing systems equipped with a 1 kN load cell. Dog-bone micro-tensile specimens were stretched at different constant cross head speed between 0.1 mm/s and 10 mm/s at room temperature. Stress at break, strain at break and strain energy density were determined in order to evaluate the healing efficiency. Data reported represent the average value from at least three samples.

Fracture tests on SENT specimens were performed at room temperature on a Zwick mechanical testing machine (model 1455) fitted with a 2 kN load cell following a single specimen J-testing experimental method [27, 33]. All the experiments were performed at room temperature. Constant cross-head separation velocity ranging from 1 mm/s to 10 mm/s were employed. Furthermore, in order to monitor the crack evolution, sample displacements and crack opening behaviours were recorded by two cameras positioned in front and to the side of the rectangular samples, respectively. To make the crack evolution easier to track, the sample surfaces near the anticipated crack path were sprayed with a white brittle paint. Fracture resistance (*J*) was estimated from the load-displacement curves obtained according to Equation 1:

$$J = \frac{\eta U}{b(w-a)}\Big|_{u} \qquad (1)$$

where *U* is the energy calculated as the area under the load-displacement curves at different levels of displacement *u*, η is the proportionality factor related to sample geometry; *b*, *w* and *a* are the

sample thickness, sample width and notch length, respectively. In the current experiments the initial crack length was about 12.5 mm, i.e. about 50% of the sample width. Given this SENT geometry, a selected value of 0.9 for η was employed [27, 29]. Subsequently, J-resistance curves functions of the crack tip opening displacement (CTOD) were derived by combining the force-displacement data with the measured CTOD evolution during the fracture tests. Resulting data were then linearly interpolated and the value of the J-integral at crack initiation (J_{Ic}), calculated at CTOD=0 mm, was used to analyse the fracture behaviour of (virgin and healed) SENT specimens. The morphology of the fracture surfaces was investigated by both a scanning electron microscope (SEM) and a confocal scanning laser microscope (LSCM) to gain further insight into the healing mechanisms. From this last experimental technique, surface roughness values were calculated as the average distance between peaks and valleys at the fracture surfaces. An increased surface roughness of the fracture surface of a healed and re-fractured samples is an indication that the healing process not only involved the reformation of physical bonds at the interface but also involved the diffusion of chains or long polymer network segments across the interface.

Dynamic mechanical thermal analysis (DMTA) experiments were conducted with a Haake™ Mars III rheometer (Thermo Scientific) in shear mode. Rectangular samples (30x8.5x3 mm) were employed for the measurement of complex modulus components as function of temperature and frequency. A shear strain amplitude within the linear viscoelastic range of 0.5% was selected; each frequency sweep scan (0.1-10 Hz) was collected at constant temperatures in a range between -25 °C and 180 °C. Storage (G') and loss (G'') modulus master curves were then generated applying the time-temperature superposition principle (TTS).

2.3 Healing efficiency measurement

The studied supramolecular elastomer, as many rubbers, exhibits a significant softening behaviour with the loading cycles. For this reason traditional healing tests used for brittle materials (i.e. healing is measured on the same specimen) are not ideal. In this work a different approach is proposed.

Healing efficiencies were determined by comparing the results obtained in tensile and fracture experiments on two sets of specimens: one with undamaged (i.e. virgin state) samples and one broken below T_g and afterwards healed at room temperature (i.e. healed state). This procedure is further described here below.

Prior to processing and testing all samples were introduced in a freezer at -20 °C overnight. This ensured all the samples to be well below their glass transition temperature (T_g= 10±2 °C, measured by DSC experiment setting a heating rate of 20 °C/min). The reference values for pristine samples tested in tensile or fracture mode were obtained from samples reheated to room temperature and equilibrated for at least 30 minutes. This yielded the values for the properties of the virgin material (P^{virgin}); where P^{virgin} are stress at break (σ_b), strain at break (ε_b) and strain energy density (W_b) for tensile tests and J-integral at crack initiation (J_{Ic}) for fracture experiments.

For the healing experiments the samples were fractured immediately after extraction from the freezer to induce brittle fracture leading to a smooth fracture surface [16], more or less perpendicular to the tensile direction After fracturing, the two separated parts of each specimen were re-positioned in shaped PTFE moulds and were laterally compressed with a constant load. Such a load was applied that the calculated contact stress across the interface between the two sample halves was about 0.1 MPa (hydrostatic condition). A schematic representation of the damage/healing steps is presented in Figure 1.

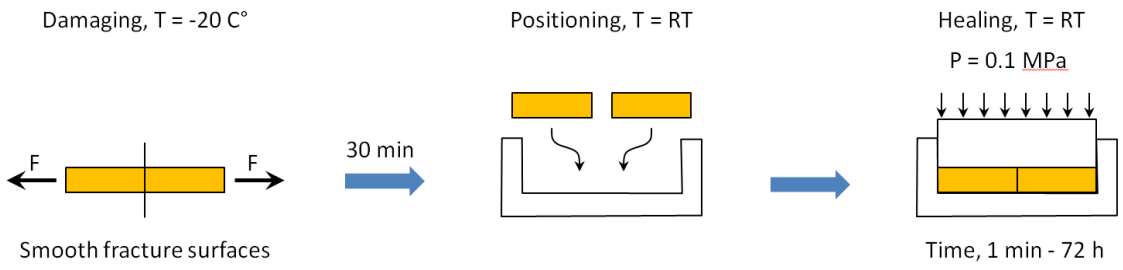

Figure 1: Schematic sequence of the fracture/healing steps applied for both tensile and fracture testing. The sample geometry is different for the two testing conditions.

After the healing treatment the samples were tested in either tensile or fracture mode and the properties of the repaired interface (P^{healed}) were obtained; where P^{healed} are the same reference parameters as in P^{virgin}. Unless otherwise specified a constant cross-head speed of 1 mm/s was employed. Contact times during healing were varied from 1 min up to 72 h. All healing and testing experiments were carried out at room temperature.

The effect of the strain rate on the healing efficiency was also investigated; both tensile and fracture experiments were performed at different cross-head velocity (0.1 mm/s - 10 mm/s) on virgin and healed samples. In this case a fixed healing time of 24 h was selected.

Healing efficiencies for the two experimental procedures were then calculated as the ratio between measured properties for healed and virgin specimens according to the usual equation:

$$Healing\ efficiency = \frac{P^{healed}}{P^{virgin}} \cdot 100 \qquad (2)$$

where P is the property of interest (failure stress, failure strain, energy at break or J-integral at crack initiation) measured at different healing time and/or different cross-head velocity.

3 Results

3.1 Tensile experiments

Representative stress-strain curves obtained in the tensile experiments for different healing time/constant rate (1 mm/s) and different cross-head speed/constant healing time (24 h) are shown in Figure 2(a) and in Figure 2(b), respectively. As can be observed, a global reduction of the mechanical properties in the damaged/repaired specimens is detected and original properties were not completely restored even for the longest healing time (Figure 2(a)). The experiments performed at different cross-head velocity show similar recovery values suggesting a nearly strain rate independent behaviour of the healing efficiency in these loading conditions. In contrast, the

mechanical response of the supramolecular elastomer showed a large strain rate sensitivity, as illustrated in Figure 2(b).

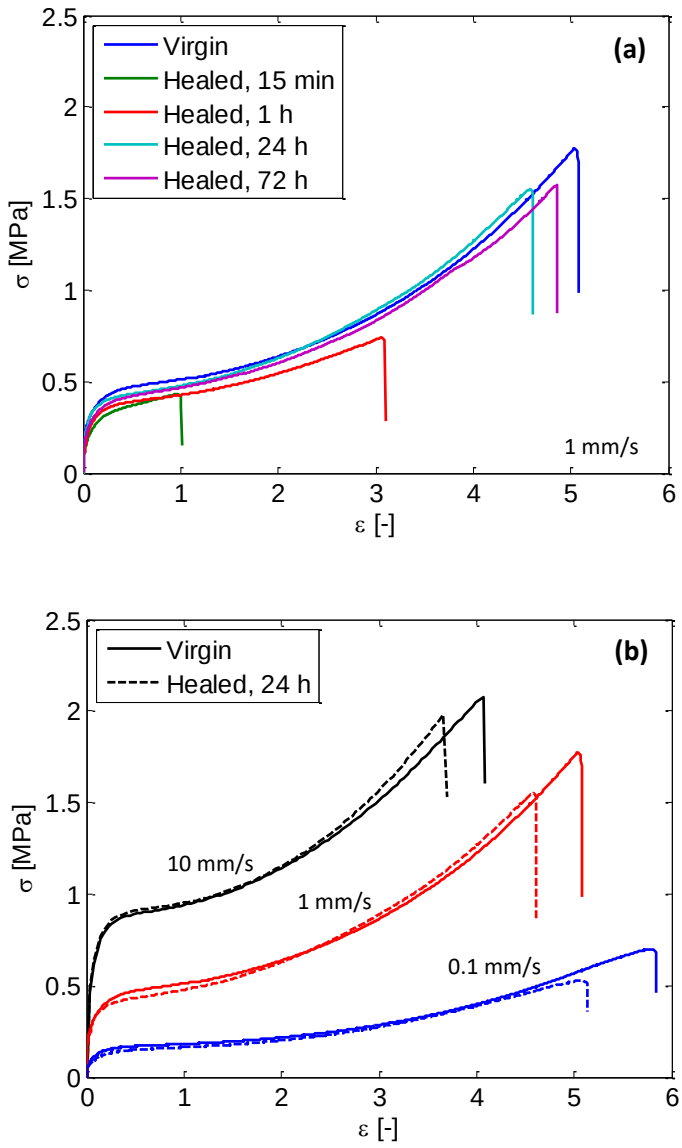

Figure 2: Stress-strain curves obtained for virgin sample and damaged samples repaired for different times tested at 1 mm/s (a) and virgin samples and damaged sample repaired for 24 h tested at different cross-head rates (b).

3.2 Fracture experiments

Examples of load-displacement curves obtained during the fracture tests performed on virgin and healed samples are presented in Figure 3(a). As in the case of tensile testing, the healed material has lower mechanical properties than the virgin one, yet a clear improvement in properties when going

from short to long healing times is detectable. For healing times longer than 24 hours no further improvement was observed. In this test, after initial loading and notch blunting, the crack starts to grow perpendicular to the applied displacement. Crack blunting and stable crack growth propagation continued up to unstable crack growth and complete separation of the tested specimens occurred. Some differences in the blunting shape were observed for virgin and healed specimens. In both cases, crack initiation was easily detectable and the evolution of the CTOD was measured through the videos obtained by the two cameras. Combining the load-displacement data and the imagine analyses the J(CTOD) curves cab be obtained (Figure 3(b)). A linear relation between J and CTOD was observed for all samples.

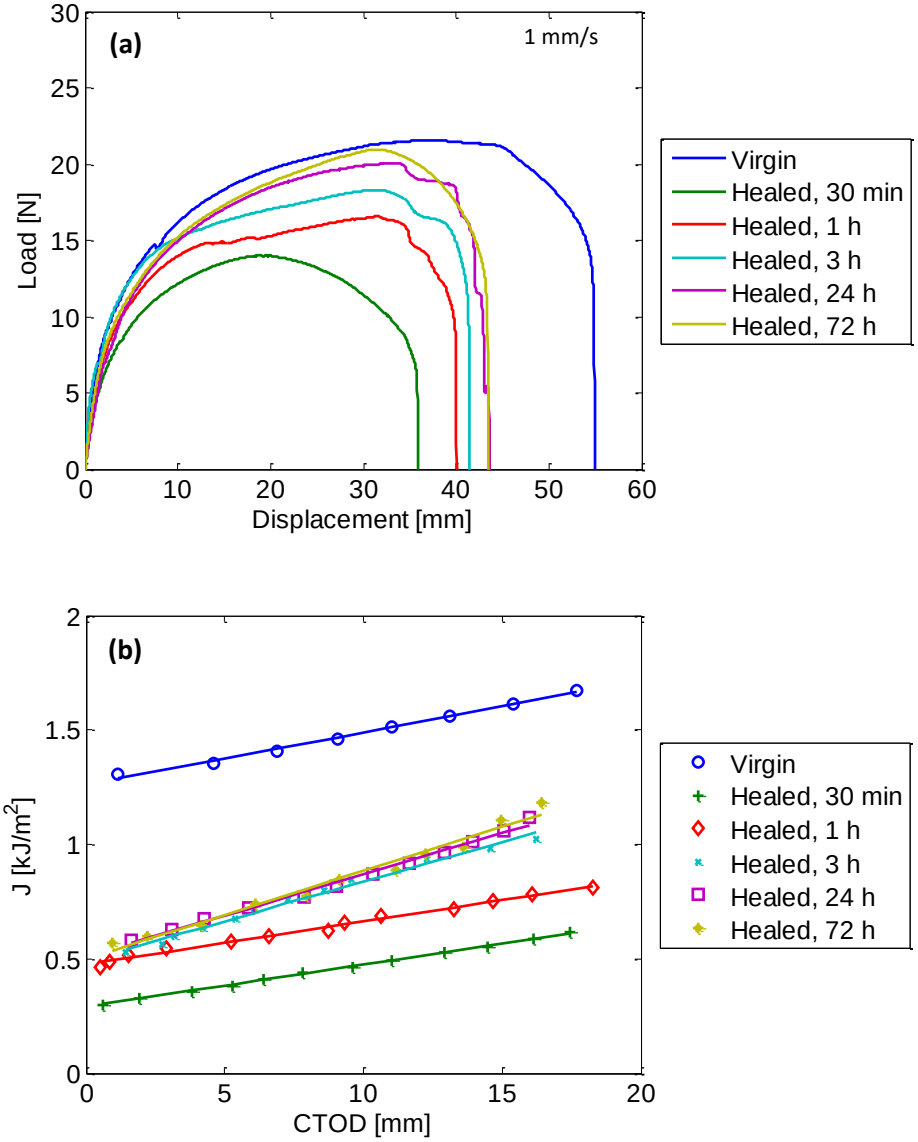

Figure 3: Load-displacement (a) and related J(CTOD) linear data fitting (b) for virgin and healed SENT samples tested at a constant cross-head velocity of 1 mm/s.

Results for constant cross-head speed (1/mms) fracture tests are summarised in Table 1. The fracture resistance at crack initiation, J_{IC}, for the virgin material is 1.26±0.15 kJ/m^2. Significantly lower values were obtained for the repaired specimens even for the longest healing time. Furthermore, analysis of the J(CTOD) data shows that the tearing modulus (T_J), calculated as the slope of the different curves, increases with healing time even exceeding the level measured for the pristine material. This experimental evidence suggested a more dissipative crack evolution process in healed samples.

Table 1: Measured average fracture properties for virgin and healed samples tested at 1 mm/s cross-head speed.

Sample	**Healing time (t) [h]**	**Critical J-integral (J_{IC}) [kJ/m^2]**	**Tearing modulus (T_J) [kJ/m^3]**
Virgin	-	1.26±0.15	23.0±1.8
Healed	0.5 (30 min)	0.29±0.06	18.5±1.5
	1	0.45±0.09	18.8±1.1
	3	0.51±0.10	34.6±1.9
	24	0.56±0.09	36.1±0.9
	72	0.57±0.07	38.5±1.3

The effect of cross-head speed on the fracture properties was also investigated. Load-displacement curves for virgin and 24 h healed samples are presented in Figure 4(a); as in the tensile experiments, a remarkable recovery of the initial strength for healed samples and a global strain rate-dependent response was observed. The pristine and repaired samples exhibited a similar J_{IC} trend as a function of cross-head velocity, however, lower J_{IC} values were measured for the healed samples (Figure 4(b)).

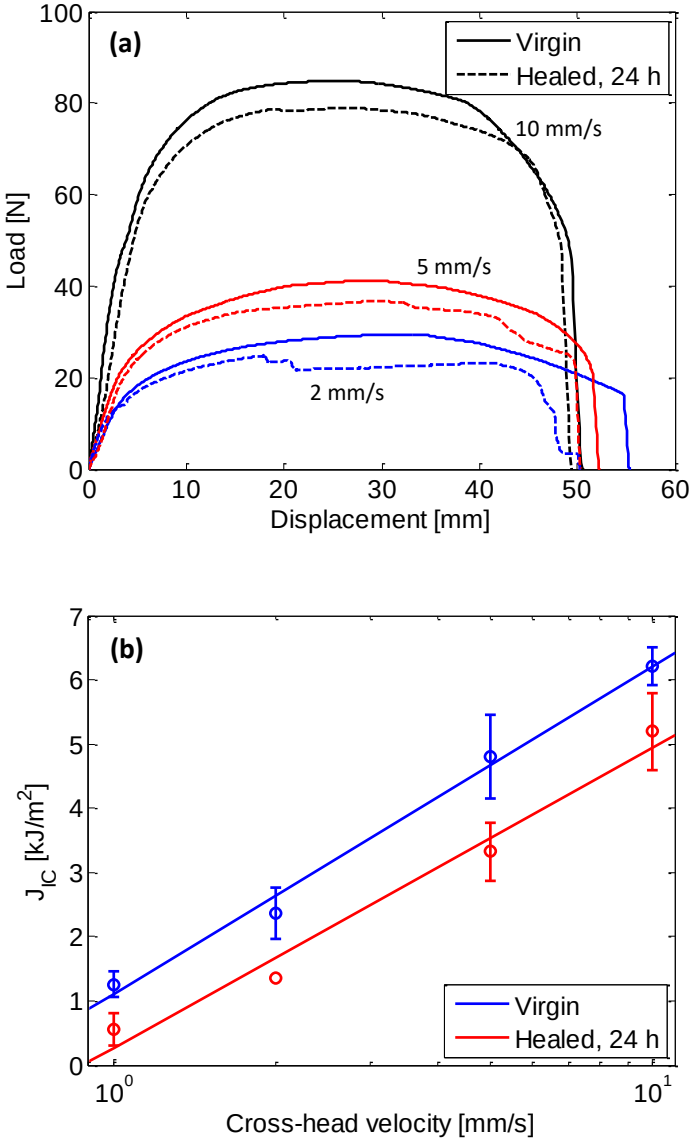

Figure 4: Load-displacement curves (a) and related fracture resistance at crack initiation (b) for virgin and healed (24 h) SENT samples tested at different cross-head velocity.

3.3 Healing efficiency measurement

As can be observed in Figure 5(a), the measured degree of healing significantly depends on the test method. While a healing efficiency of around 90% healing is obtained in tensile mode (σ_b recovery), a healing efficiency of only 40% is obtained in fracture mode at the lowest constant cross-head velocity (1 mm/s). Different healing kinetics were detected for the two testing procedure: in fracture mode, the maximum healing level is reached at shorter healing times than in tensile testing. Comparable results in the healing efficiency in tensile mode were obtained for the other critical parameters

selected for healing measurement (ε_b and W_b). The same rate of recovery is observed and after 24 h healing a maximum recovery of all original tensile properties is achieved.

Tensile tests performed on 24 h healed samples revealed a slight influence of the cross-head rate on the measured healing efficiency (Figure 5(b)). Conversely, in fracture experiments a marked increment of the recovery performances with the deformation rate was detected; in particular a healing level (~80%) close to the value measured in tensile mode was only reached at the highest cross-head speed.

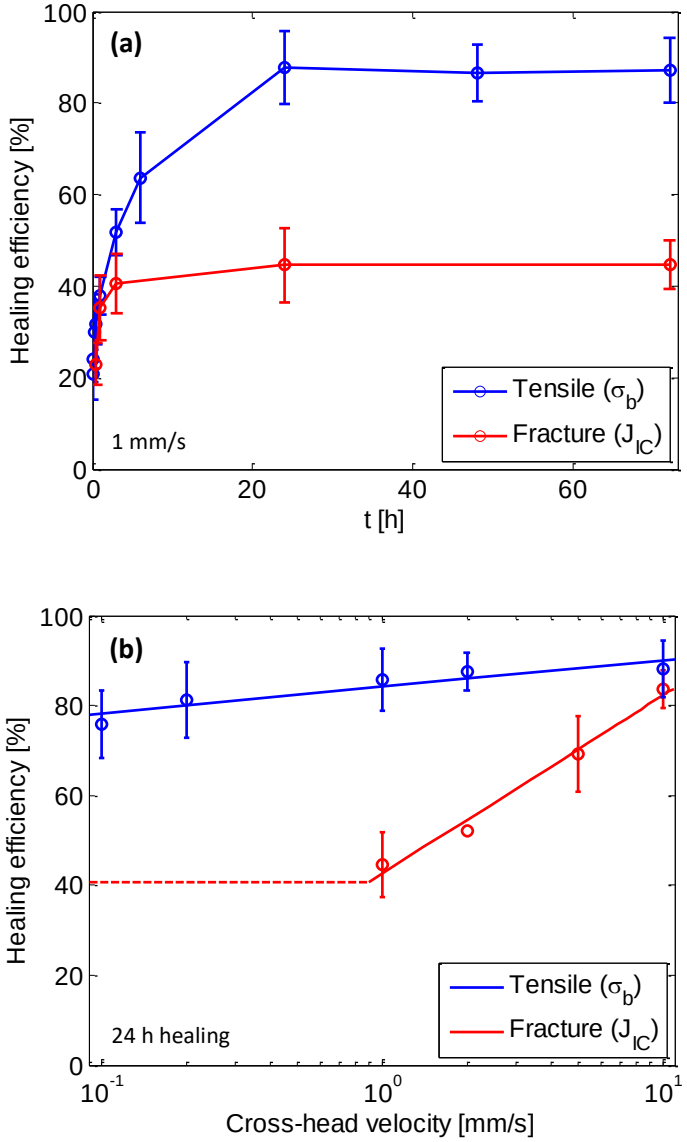

Figure 5: Healing efficiency calculated for tensile and fracture experiments as a function of healing time (a) and of cross-head velocity (b).

4 Discussion

Tensile and fracture experiments on virgin and healed samples led to different measured healing performances showing a difference in the recovery of original properties depending on the testing conditions. However the properties measured in the two tests all depend on the same chemical, physical and topological characteristics of the polymeric network at the interface [34].

A first physical model, describing the time evolution of the new polymer arrangements and the related mechanical properties of the healed interface, was developed by Wool et al. [35, 36]; this model takes into account surface rearrangement and approach, wetting, chain inter-diffusion and randomization. Taking the proposed double random walk process as a mathematical representation for the actual molecular rearrangement at the two fracture surfaces the result of the healing treatment can best be analysed on a time scale of $t^{0.25}$ (where t is healing time). The results are shown in Figure 6 and, focusing on tensile experiments, three distinct regions can be individuated: (i) for short healing times, up to 5 min, mechanical properties evolve negligibly; (ii) greater repair times (from 5 min to 24 h) lead to an increase of σ_b up to a critical level (iii) where no additional increment is observed. This behaviour can be descripted by the following equation:

$$\sigma_b(t) = \begin{cases} \sigma_0 & \text{if } t < 5\,\text{min} \\ Kt^{0.25} & \text{if } 5\,\text{min} < t < 24\,\text{h} \\ \sigma_\infty & \text{if } t > 24\,\text{h} \end{cases} \qquad (3)$$

where σ_0 and σ_∞ are the failure stress measured for the shortest and longest healing time, respectively, *K* is a parameter depending on the total number of chain constraints per unit volume and on the chain diffusion coefficient [35].

The fracture test data show a slightly different behaviour yet the plateau in the measured recovered properties is also reached after about 24 h.

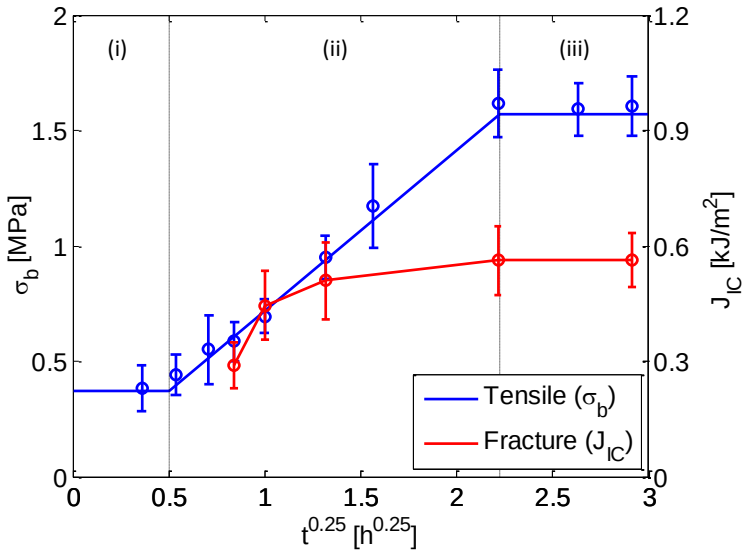

Figure 6: Evolution of stress at break and fracture resistance at crack initiation for different healing time.

Some insight into the different processes involved in the polymer interface healing and their time evolution can be deduced analysing these results. The three individuated steps in the recovery of mechanical properties can be then related to the different phenomena. In the first stage, thanks to an optimal surfaces contact ensured by low temperature fracture, wetting process rapidly took place; hydrogen bonds re-association at the interface is then responsible for the initial mechanical properties recovering promoting the following healing steps. Chain inter-diffusion may start at this stage, however its effect on the mechanical properties is still marginal due to the short diffusion distance at the interface [37]. Conversely, in the second region, the longest healing times allow large chain movements through the polymer/polymer interface. Physical and topological chain constraints formation is then possible leading to the measured strength increment. Moreover, the additional hydrogen bonds, which can be formed as a result of the chain inter-diffusion, may affect the healing process. Their formation contributes to the material strength recovery, however a reduction in the dynamics of the polymer chains cannot be excluded [38, 39].

The measured healing performances between tensile and fracture experiments suggest a difference in the failure mode of the repaired material. In both experiments the crack evolution at the healed interface occurs by disentanglement of the minor chains or by chains scission [23, 40]. In all tensile

tests performed at different deformation rate, polymer chains are globally stretched and when the local stress exceeds a critical level, a deformation zone with a marked anisotropy, containing mixtures of partially interpenetrating or entangled chains, is generated [41]. Subsequently fracture propagates and its rate is dominated by bond rupture. At high cross-head displacement rate the constrained chains having crossed the interface and diffused into the opposite sample half act like cross-linked ones. In this condition, the healed interface can exhibit mechanical properties close to the pristine material. On the other hand, for low cross-head displacements rates the crack propagates slowly and the competition between chain scission and chain pull-out is more prominent. In these conditions, chains slip promoting their pull-out at the interfaces takes place; thus, the higher T_J observed for the healed SENT samples may be related to this process being consistent with the nature of the physical bonds and chain constraints reformed at the fracture plane.

The evolution of fracture properties with deformation rate observed for the virgin and healed material can be better understood by examining the rheological behaviour of the supramolecular polymer. The storage shear (G') and the loss shear modulus (G'') over a wide frequency range resulting from the rheological experiments and subsequent TTS analysis are plotted in Figure 7. At intermediate frequencies, viscous response exhibited by the material promoted the flow behaviour of the polymer network; dissipative events such as slip between polymer chains or chain disentanglement can occur. On the other hand, at higher frequencies (short time scale), the elastic component dominated the mechanical response of the material: rearrangement and relaxation processes of the polymer network are less effective and the physical constraint between the polymer chains act as apparent cross-links. A transition between these material response is individuated at a characteristic frequency (f_c) of ~1.9 Hz as the crossover point between G' and G''; the resulting characteristic time (τ_c) of ~0.5 s, calculated as the inverse of f_c, is in the same timescale range of crack propagation phenomena in fracture experiments (from 2 s to 40 s for the highest and the lowest cross-head velocity, respectively) giving a possible explanation for the rate dependent fracture properties of both virgin and healed material. At the lower frequencies the storage modulus

reaches again a plateau, an indication of the existence of a permanent (non-reversible) covalent network. This is in line with the fracture tests suggesting the impossibility of a full restoration of the interface as the irreversible network cannot be reformed during the healing process.

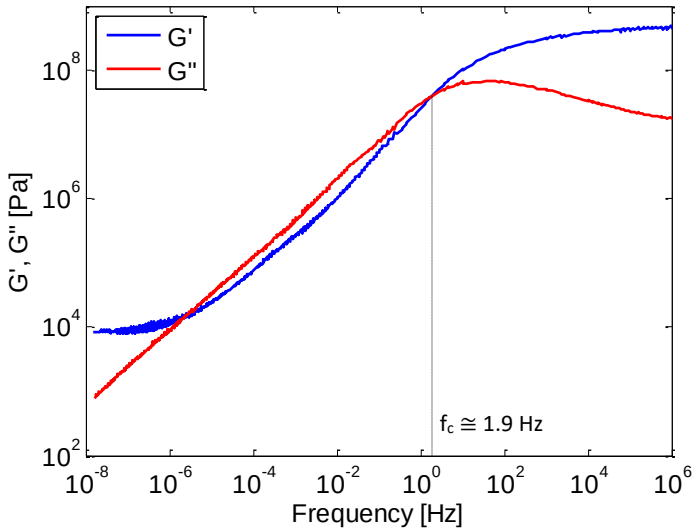

Figure 7: G' and G'' master curves (25 °C) obtained from DMTA analysis.

The hypothesis of chain inter-diffusion through the polymer/polymer interface during the healing process could be further supported by image analysis of the fracture surfaces obtained for SENT samples tested in various experimental conditions. As shown in Figure 8 (SEM analysis) and Figure 9(a) (surface profiles), the fracture surfaces for the pristine sample broken at a low temperature and the fracture surfaces of healed surfaces (re-fractured at room temperature) exhibited different morphologies. In particular, the initial low temperature fracture surface and the one healed for a short time showed a flat and smooth fracture plane (Figure 8(a),(c)). On the other hand, wavy fracture surfaces were observed for both RT fractured and long healing time samples (Figure 8(b),(d)). The fracture surface roughness evolution with the healing time confirmed a partial recovery of the pristine material properties (Figure 9(b)). It is very interesting to note that the time at which the surface roughness increased significantly with respect to the roughness of the initial fracture surface corresponds very well with the minimal time required to reach the recovery of the fracture

toughness. The development of a surface roughness is indicative of the chain density and total bond strength across the healed interface locally reaching such high values that fracture test induced a wavy crack path comparable to the one observed for the virgin material. Creation of surface roughness is an indication of a more substantial healing action that pure recovery of the tensile strength. The use of the surface roughness as an indicator of the healing process as demonstrated here is new may also be informative for other self-healing systems, in which the initial fracture surface is relatively smooth.

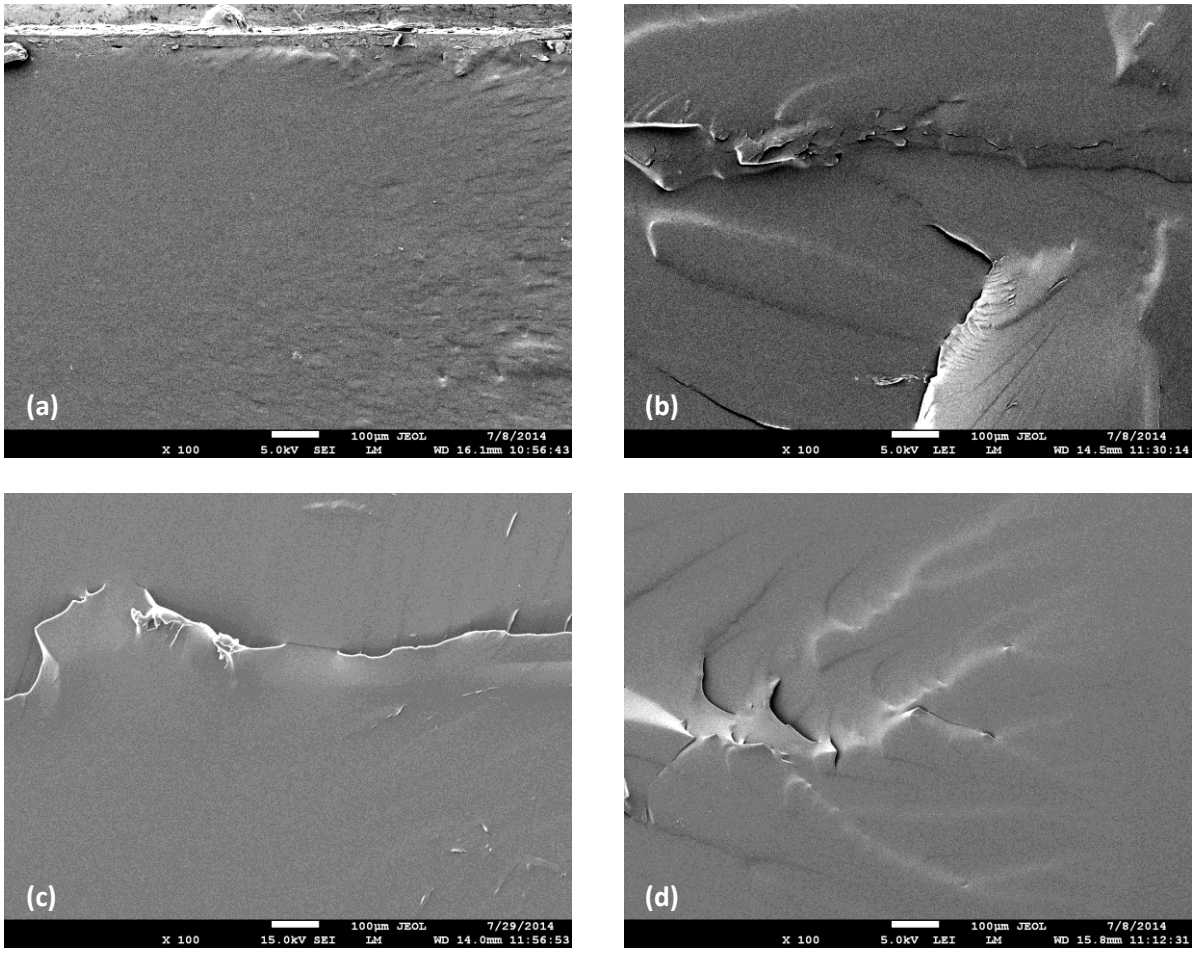

Figure 8: Micrographs of fracture surfaces obtained at low temperature (a) and room temperature (b) for the virgin material and arising from fracture experiments on repaired samples after 30 min (c) and 24 h (d) healing time.

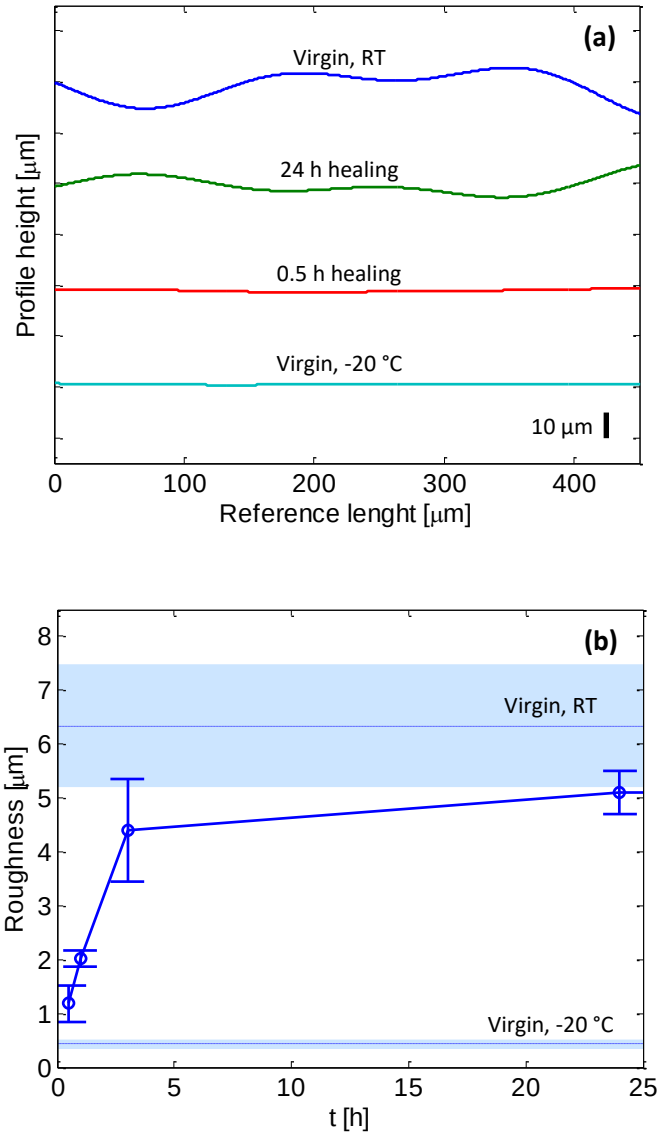

Figure 9: Representative fracture surfaces profiles for samples tested in different experimental conditions (a) and related surface roughness evolution with healing time (b).

From these results is becomes clear that the restoration of physical bonds at the interface does not lead to a complete healing, which can only be reached when the new interface region has the same network conformation statistics as the bulk material. For any elastomeric material consisting of a stronger permanent covalent network and weaker dynamic network such a partial recovery is unavoidable. The research presented here makes it clear that the almost complete recovery of mechanical properties under tensile testing at relatively higher deformation speed gives a misleading impression of the actual recovery of structure and properties across the interface. The fracture

mechanics experiments reflect the partial nature of the healing even after long annealing times more clearly. However, the tensile test results made it easier to separate the different stages involved in the healing process.

5 Conclusions

The degree of healing as measured by tensile and fracture mechanical testing of a supramolecular elastomer was demonstrated to be rather different yet to follow the same time dependence. While the tensile tests showed an almost complete recovery of the initial properties for all straining rates, the recovery of the fracture mechanical properties was only 40% for the lowest deformation rate. For conditions leading to substantial recovery of the fracture mechanical properties an increase in the fracture roughness with respect to that of the original fracture surface was measured. The combination of the two mechanical testing methods in combination with rheological and surface roughness measurements allowed a clearer separation of the processes taking place during healing. The results presented here suggest that the fracture procedure provides a more reliable measurement of the real degree of healing (defined as the recovery of the original polymer network). Since not all chemical bonds are reformed across the healed fracture surface, a full recovery of all mechanical properties for a hybrid polymer network based supramolecular elastomer by annealing at room temperature is impossible even though the strength of healed samples as measured in a tensile test can reach the same value as that of the undamaged pristine material.

Acknowledgments

This research has been supported by the European Seventh Framework Programme, NMP-2012-2.1-3, SHINE project - grant agreement 309450. The authors are grateful to Arkema for having supplied the material and thank Dr. J. P. Disson (Arkema) for the helpful discussions.

References

1. Hager, M.D., et al., *Self-healing materials.* Advanced Materials, 2010. **22**(47): p. 5424-5430.
2. Garcia, S.J., *Effect of polymer architecture on the intrinsic self-healing character of polymers.* European Polymer Journal, 2014. **53**(1): p. 118-125.
3. Sijbesma, R.P., et al., *Reversible polymers formed from self-complementary monomers using quadruple hydrogen bonding.* Science, 1997. **278**(5343): p. 1601-1604.
4. Cordier, P., et al., *Self-healing and thermoreversible rubber from supramolecular assembly.* Nature, 2008. **451**(7181): p. 977-980.
5. Zhang, A., et al., *Self-healing supramolecular elastomers based on the multi-hydrogen bonding of low-molecular polydimethylsiloxanes: Synthesis and characterization.* Journal of Applied Polymer Science, 2013. **129**(5): p. 2435-2442.
6. Lafont, U., H. Van Zeijl, and S. Van Der Zwaag, *Influence of cross-linkers on the cohesive and adhesive self-healing ability of polysulfide-based thermosets.* ACS Applied Materials and Interfaces, 2012. **4**(11): p. 6280-6288.
7. AbdolahZadeh, M., et al., *Healable dual organic–inorganic crosslinked sol–gel based polymers: Crosslinking density and tetrasulfide content effect.* Journal of Polymer Science Part A: Polymer Chemistry, 2014. **52**(14): p. 1953-1961.
8. Varley, R.J. and S. van der Zwaag, *Autonomous damage initiated healing in a thermo-responsive ionomer.* Polymer International, 2010. **59**(8): p. 1031-1038.
9. Grande, A.M., et al., *Rate-dependent self-healing behavior of an ethylene-co-methacrylic acid ionomer under high-energy impact conditions.* Journal of Applied Polymer Science, 2013. **130**(3): p. 1949-1958.
10. Rhaman, M.A., et al., *Self-healing behavior of blends based on ionomers with ethylene/vinyl alcohol copolymer or epoxidized natural rubber.* Macromolecular Materials and Engineering, 2011. **296**(12): p. 1119-1127.
11. Rahman, M.A., et al., *Self-repairing systems based on ionomers and epoxidized natural rubber blends.* ACS Applied Materials and Interfaces, 2011. **3**(12): p. 4865-4874.
12. Rekondo, A., et al., *Catalyst-free room-temperature self-healing elastomers based on aromatic disulfide metathesis.* Materials Horizons, 2014. **1**(2): p. 237-240.
13. Herbst, F., et al., *Self-healing polymers via supramolecular forces.* Macromolecular Rapid Communications, 2013. **34**(3): p. 203-220.
14. Tournilhac, F., et al., *Self-healing supramolecular networks.* Macromolecular Symposia, 2010. **291-292**(1): p. 84-88.
15. Binder, W.H., *Self-Healing Polymers: From Principles to Applications*. 2013, Weinheim, Germany: Wiley-VCH.
16. Maes, F., et al., *Activation and deactivation of self-healing in supramolecular rubbers.* Soft Matter, 2012. **8**(5): p. 1681-1687.
17. Rahman, M.A., et al., *Autonomic Self-Healing in Epoxidized Natural Rubber.* ACS Applied Materials & Interfaces, 2013. **5**(4): p. 1494-1502.
18. Rahman, M.A., et al., *Role of phase morphology on the damage initiated self-healing behavior of ionomer blends.* Macromolecular Materials and Engineering, 2013. **298**(12): p. 1350-1364.
19. Keller, M.W., S.R. White, and N.R. Sottos, *A self-healing poly(dimethyl siloxane) elastomer.* Advanced Functional Materials, 2007. **17**(14): p. 2399-2404.
20. Keller, M.W., S.R. White, and N.R. Sottos, *Torsion fatigue response of self-healing poly(dimethylsiloxane) elastomers.* Polymer, 2008. **49**(13-14): p. 3136-3145.
21. Hamed, G.R., *Molecular Aspects of the Fatigue and Fracture of Rubber.* Rubber Chemistry and Technology, 1994. **67**(3): p. 529-536.
22. Cristiano, A., et al., *Fracture of model polyurethane elastomeric networks.* Journal of Polymer Science, Part B: Polymer Physics, 2011. **49**(5): p. 355-367.

23. Brown, H.R., *The adhesion of polymers: Relations between properties of polymer chains and interface toughness.* Journal of Adhesion, 2006. **82**(10): p. 1013-1032.
24. Rivlin, R.S. and A.G. Thomas, *Rupture of rubber. I. Characteristic energy for tearing.* Journal of Polymer Science, 1953. **10**(3): p. 291-318.
25. Cherepanov, G.P., *Crack propagation in continuous media: PMM vol. 31, no. 3, 1967, pp. 476–488.* Journal of Applied Mathematics and Mechanics, 1967. **31**(3): p. 503-512.
26. Rice, J.R., *A Path Independent Integral and the Approximate Analysis of Strain Concentration by Notches and Cracks.* Journal of Applied Mechanics, 1968. **35**(2): p. 379-386.
27. Ramorino, G., et al., *Investigation of fracture resistance of natural rubber/clay nanocomposites by J-testing.* Engineering Fracture Mechanics, 2010. **77**(10): p. 1527-1536.
28. Naït-Abdelaziz, M., et al., *J integral as a fracture criterion of rubber-like materials using the intrinsic defect concept.* Mechanics of Materials, 2012. **53**: p. 80-90.
29. Agnelli, S., et al., *Fracture resistance of rubbers with MWCNT, organoclay, silica and carbon black fillers as assessed by the J-integral: Effects of rubber type and filler concentration.* Express Polymer Letters, 2012. **6**(7): p. 581-587.
30. Montarnal, D., et al., *Epoxy-based networks combining chemical and supramolecular hydrogen-bonding crosslinks.* Journal of Polymer Science, Part A: Polymer Chemistry, 2010. **48**(5): p. 1133-1141.
31. Montarnal, D., et al., *Versatile one-pot synthesis of supramolecular plastics and self-healing rubbers.* Journal of the American Chemical Society, 2009. **131**(23): p. 7966-7967.
32. Montarnal, D., et al., *Synthesis of self-healing supramolecular rubbers from fatty acid derivatives, diethylene triamine, and urea.* Journal of Polymer Science, Part A: Polymer Chemistry, 2008. **46**(24): p. 7925-7936.
33. Kim, B.H. and C.R. Joe, *Single specimen test method for determining fracture energy (Jc) of highly deformable materials.* Engineering Fracture Mechanics, 1989. **32**(1): p. 155-161.
34. Gent, A.N. and W.V. Mars, *Chapter 10 - Strength of Elastomers*, in *The Science and Technology of Rubber (Fourth Edition)*, J.E. Mark, B. Erman, and C.M. Roland, Editors. 2013, Academic Press: Boston. p. 473-516.
35. Wool, R.P. and K.M. O'Connor, *A theory of crack healing in polymers.* Journal of Applied Physics, 1981. **52**(10): p. 5953-5963.
36. Kim, Y.H. and R.P. Wool, *A theory of healing at a polymer-polymer interface.* Macromolecules, 1983. **16**(7): p. 1115-1120.
37. Wool, R.P., *Properties and Entanglements of Amorphous Polymer Interfaces.* Journal of Elastomers and Plastics, 1985. **17**(2): p. 106-118.
38. De Lucca Freitas, L.L. and R. Stadler, *Thermoplastic elastomers by hydrogen bonding. 3. Interrelations between molecular parameters and rheological properties.* Macromolecules, 1987. **20**(10): p. 2478-2485.
39. de Lucca Freitas, L. and R. Stadler, *Thermoplastic elastomers by hydrogen bonding 4. Influence of hydrogen bonding on the temperature dependence of the viscoelastic properties.* Colloid & Polymer Science, 1988. **266**(12): p. 1095-1101.
40. Ge, T., et al., *Healing of polymer interfaces: Interfacial dynamics, entanglements, and strength.* Physical Review E, 2014. **90**(1): p. 012602.
41. Wool, R.P., *Self-healing materials: A review.* Soft Matter, 2008. **4**(3): p. 400-418.